2

THEORETICAL CONCEPTS

"The experiment left no doubt that, as far as accuracy of measurement went, the resistance disappeared. At the same time, however, something unexpected occurred. The disappearance did not take place gradually but abruptly. From 1/500 the resistance at 4.2K, it could be established that the resistance had become less than a thousand-millionth part of that at normal temperature. Thus the mercury at 4.2K has entered a new state, which, owing to its particular electrical properties, can be called the state of superconductivity."

- Heike Kamerlingh Onnes-

Contents

2.1 Superconductivity

When a superconductor is cooled down below its critical temperature T_c, the electrical resistance drops to absolute zero. This is probably the most striking property of superconducting materials. In general, the electrical resistance of a metal is originated by three independent mechanisms: i) electron-electron interactions, ii) electron-phonon interactions, and iii) interactions of the electrons with impurities, crystallographic defects or grain boundaries. Since the mechanisms are independent, they contribute to the resistivity in an additive way. The contribution from impurities, defects an grain boundaries ρ_{imp} is basically temperature independent, the one due to electron-electron interaction $\rho_{\text{el-el}}$ is proportional to T^2 while the electron-phonon contribution $\rho_{\text{el-ph}}$, instead, increases with increasing the temperature as T^5. At low temperatures the latter term is therefore negligible and the temperature dependence of the resistivity is given by

$$\rho(T) = \rho_0 + aT^2 + ... \tag{2.1}$$

where the first and the second term are respectively ρ_{imp} and $\rho_{\text{el-el}}$. This typical behavior is shown in Fig.2.1 (dashed line). Thus the ratio between resistivity at room

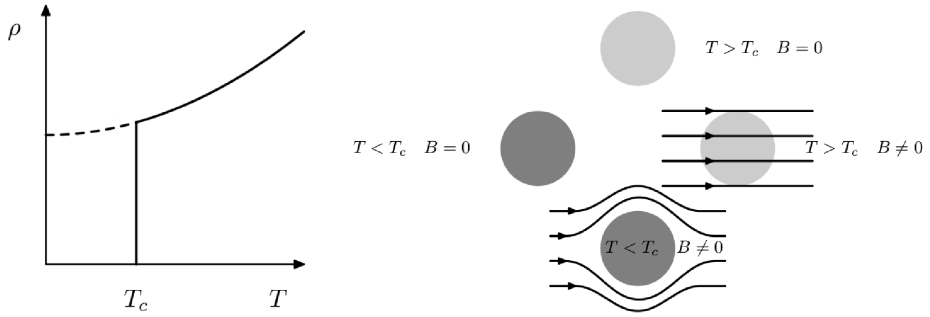

Figure 2.1: (Left) Low temperature dependence of the resistivity for a normal metal (dashed line) and for a superconductor (full line). Above T_c the behavior is the same. (Right) The Meissner-Ochsenfeld effect in a superconductor: both if the superconductor is cooled down in field (middle right sketch) or with zero field (middle left), when $T < T_c$ the magnetic field cannot penetrate the superconductor (bottom). From Ref. [1].

temperature and at low temperature ($\rho_{300\text{K}}/\rho_{0\text{K}}$), called the residual-resistivity ratio (RRR), is a measure of the purity of the metal. Kamerling Onnes, with his measurements at low temperatures, aimed to experimentally prove this model and refute alternative theories proposed at the time. The drop to zero resistance came completely

unexpected. A typical superconducting transition is shown in sketched in Fig.2.1 (full line).

The other characterizing property of a superconductor is the exhibition of the Meissner-Ochsenfeld effect. If the superconductor is cooled down in a (small) magnetic field, the field is expelled at the transition to the superconducting state. So, a superconductor is not simply a perfect conductor but also a perfect diamagnet. The occurrence of the Meissner effect for a material of interest is often used as a definitive proof of bulk superconductivity. As a matter of fact, the magnetic field is not completely screened but it penetrates the surface of the superconductor over a characteristic short length given by the penetration depth λ. The field inside the superconductor is given by $B = B_0 e^{-x/\lambda}$, with x the distance from the surface. λ is typically of the order of a few tens of nanometers.

An understanding of the microscopical mechanism of superconductivity was missing for several years after its experimental discovery. Superconductivity was first described phenomenologically in 1935 by the London theory. The description, similar to superfluidity in ^{4}He, used a two-fluid model: the current density $\mathbf{j}$ results from the sum of two components, $\mathbf{j}_\mathrm{n}$ and $\mathbf{j}_\mathrm{s}$; $\mathbf{j}_\mathrm{n}$ is the normal component which carries entropy, so disorder and heat; $\mathbf{j}_\mathrm{s}$ is the superfluid component, which is ordered and does not carry heat. The total density of carriers $n = n_\mathrm{n} + n_\mathrm{s}$ is constant and the relative density of carriers for the two components, n/n_n and $n_\mathrm{s}/n = 1 - n_\mathrm{n}/n$, varies with the temperature. In the normal state only the normal component is present. When reducing the temperature the superconducting component increases, shorting the normal carriers. This simple model leads to the London equation, which connects the current density $\mathbf{j}$ with the vector potential $\mathbf{A}$,

$$\mathbf{j} = -\frac{n_\mathrm{s} e^2}{m_e}\mathbf{A}, \tag{2.2}$$

where e and m_e are the charge and the mass of the electron. Eq.2.2 is valid in the regime when the penetration depth λ is larger than the effective coherence length ξ. The effective coherence length is obtained by combining ξ_0, the characteristic coherence length of the superconducting state, and the mean free path ℓ, via the relation

$$\frac{1}{\xi} = \frac{1}{\xi_0} + \frac{1}{\ell}. \tag{2.3}$$

Pippard introduced a generalized form of Eq.2.2, in order to include the cases when $\lambda < \xi$. The London theory is a very simple phenomenological model and was based on the introduction of two equations, in addition to Maxwell's equations, which could describe perfect diamagnetism and zero resistance. Although the model did not ex-

plain the microscopical origin of superconductivity, it proved to be very powerful and in many cases it gives the right predictions. The equation, furthermore, was later derived by Bardeen, Cooper and Schrieffer starting from a full microscopical quantum theory.

2.1.1 BCS vs Ginzburg-Landau theory

A microscopical description of superconductivity was proposed by Bardeen, Cooper and Schrieffer in 1957 and it is known as BCS theory. Their model was developed based on several experimental observations, such as the decrease of Gibbs energy and entropy when going to the superconducting state, the quantization of the magnetic flux with a charge equal to $2e$ and the exponential dependence of the specific heat. These observations suggested that the superconducting state was an ordered state, with the electrons paired up in two, and "protected" by an energy gap. According to the BCS theory, when the temperature is reduced to the critical value, the electrons start to feel an attractive force and they pair up in Cooper pairs. Indeed, the Cooper principle states that if there is an attractive interaction, however weak, between electrons excited above the Fermi energy E_F, there exists a pair bound state lower than E_F separated by an energy gap Δ from E_F. The attraction between electrons is possible, despite the repulsive Coulomb interaction, thanks to the mediation of the phonons. An electron moving in the lattice attracts the surrounding positively charged ions, which slightly move from their original position in the lattice. The positively charged cloud left behind by the first electron, attracts the second electron. As a result there is an attractive force between the two electrons. The coupled electrons have opposite momentum and, because of the Pauli principle, opposite spin. So, both the total momentum and the total spin of a Cooper pair are zero and the pair has a bosonic-like behavior. When there is a superconducting transition, like in a Bose-Einstein condensation, the Cooper pairs condense to one common ground state. Since now the interaction with the impurities does not happen with a single electron but with the whole condensate of cooperative electrons, a larger energy is needed to excite a single particle (quasiparticle). Indeed, the ground state is separated from the first excited state by an energy gap 2Δ. In general, the superconducting coupling is weak, and that is why superconductivity appears only at low temperatures, when the thermal energy is low. The magnitude of the coupling, proportional to Δ, typically does not exceed a few meV. Δ also defines the size of a Cooper pair, the coherence length ξ_0, which is given by

$$\xi_0 = \frac{\hbar v_F}{\pi \Delta}, \tag{2.4}$$

where $\hbar$ is the reduced Planck constant and v_F is the Fermi velocity.

An alternative way to describe superconductivity is via the Ginzburg-Landau (GL) model, which was introduced in 1950 [2]. GL is a phenomenological macroscopic description of superconductivity which does not explicitly include the microscopic origin of the phenomenon. Nonetheless, Gor'kov [3] some years later could show that it is possible to microscopically derive the GL model from the BCS theory, confirming its validity. The Ginzburg-Landau theory is based on the observation that in superconductivity there is a phase transition: as for the transition water-vapor, the two states of normal conductance and superconductivity are considered two separate phases. For this reason, the GL theory is accurate close to T_c and become less precise at lower temperatures. The other important aspect is that when a material becomes superconducting, it goes to a more ordered state, associated with a symmetry breaking. In systems where such symmetry breaking occurs, we can define an order parameter which is zero in the disordered state and emerges when crossing the transition. An example of symmetry breaking occurs in ferromagnets, when the temperature is lowered below the Curie temperature and the spins become aligned in the ordered magnetized state, along a defined direction. In this case the order parameter is the magnetization. In the GL model a complex order parameter Ψ is associated with the strength of superconductivity. $\Psi = 0$ in the normal state and $\Psi(T) \neq 0$ in the superconducting state. By deriving the GL theory starting from the microscopic BCS, it is possible to show that Ψ has the physical meaning of the wave function describing the condensate where $|\Psi(T)|^2$ is the density of Cooper pairs. There is also a phase connected to the wave function, which leads to the phenomenon of flux quantization. Currents, in this formalism, are driven by phase differences. The formalism of GL is very powerful. It can explain the Meissner-Ochsenfeld effect and it allows to describe complex problems without addressing the microscopic details. Examples where the GL theory is particularly useful is the description of vortices in type-II superconductors (see Sec.2.1.3) and the proximity effect between a superconductor and a different material (see Sec.2.2). The GL coherence length is defined as

$$\xi_{GL}(T) = \sqrt{\frac{\hbar^2}{4m|\alpha(T)|}}, \tag{2.5}$$

where m is the effective mass of the electron and $\alpha(T)$ the coefficient of the $|\Psi|^2$ in the expression of the free energy. $\xi_{GL}(T)$ has the meaning of the length scale of the spatial variation of the order parameter Ψ. The temperature dependence can be made explicit by $\xi_{GL}(T) = \xi(0)\sqrt{1/(T/T_c - 1)}$, where $\xi(0)$ is equivalent to the coherence length

defined in Eq.2.4.

2.1.2 A modern description: the Usadel equation

Both the original BCS and GL theories have some limitations. The GL model is limited to a temperature regime close to T_c, as already pointed out in the previous section, and it is valid only in conditions of equilibrium. The BCS model, on the other hand, is valid at zero temperature (also in equilibrium) and neglects all the interactions other than the attractive Cooper pairing. In real experiments the temperature is typically finite, not necessarily close to T_c, and interactions such as scattering with impurities, electron-phonon or electron-electron interactions, play an important role. This is another way of saying that quasiparticle excitations are difficult to handle, as are situations when the material parameters change rapidly, as for instance at interfaces.

In order to describe real experiments, thus, the Bogoliubov-de Gennes equation (BdG), based on the BCS theory, seems to be more suitable. In the BCS the Hamiltonian of the system is written in terms of creation and annihilation operators for single particle states (Bloch waves with a defined momentum and spin). However, in the superconducting state the excitations are quasiparticles which originate from the breaking of Cooper pairs. For this reason, instead of single particle states, it is more correct to consider mixed states of electrons and holes. This concept, first introduced by Bogoliubov, was developed further in the BdG equation [4], given by

$$\begin{pmatrix} H_0 & \Delta(r) \\ \Delta(r)^* & -H_0^* \end{pmatrix} \begin{pmatrix} \psi_e(r) \\ \psi_h(r) \end{pmatrix} = E \begin{pmatrix} \psi_e(r) \\ \psi_h(r) \end{pmatrix}. \tag{2.6}$$

Here the eigenfunctions $\psi_e(r)$ and $\psi_h(r)$ are the electron-like and hole-like part of the wave function, respectively, Δ is the superconducting pair potential, H_0 the Hamiltonian of the system and E the energy (eigenvalue) of the excitations. It is interesting to notice that only when $\Delta \neq 0$, thus below T_c, there is a mixing between $\psi_e(r)$ and $\psi_h(r)$, which are decoupled otherwise. H_0, beside the kinetic energy term, includes all the interactions different from the pairing potential, such as for example the scattering with impurities, defects or grain boundaries. However, even if it seems that the BdG equations could be used to describe diffusive systems, in practice it is not applicable. Indeed, in order to find a solution we should know in details the scattering potential, namely the exact position of all the impurities an defects. In addition, the resulting diffraction effects on the **k** vectors of the scattered electrons would be on the length scale of the Fermi wave length λ_F, at least two orders of magnitude smaller than

the superconducting characteristic length ξ_S. In most of the cases, the study of such small scale effects in a mesoscopic goes beyond the computational capability and a the BdG equation cannot be solved.

A solution to the problem is found by introducing the formalism of the Green's functions, "borrowed" from the quantum field theory. In this formalism, instead of calculating directly the amplitude of the wave functions, as done by the BdG equation, the expectation values of the moving charges are probed. The (normal) Green function $G(x,t;x',t')$ expresses the probability of moving an electron from a position x' at the time t' to a position x at the time t. This is done by "creating" a charge at (x',t') with the Heisenberg creation operator $\Psi^\dagger(x',t')$ and "removing" it at (x,t) with the annihilation operator $\Psi(x,t)$. The operation is then averaged on all the possible paths of the charge from (x',t') to (x,t),

$$G(x,t;x',t') = \langle \Psi(x,t)\Psi^\dagger(x',t') \rangle . \tag{2.7}$$

In this way, the G function basically describes the transport properties of the system. If G is fully known, it is possible to estimate many properties of the system. In the limit $(x,t) \Rightarrow (x',t')$, for example, it gives the local density of states, while its spatial derivative gives the electrical current. G describes the transport of single electrons. In case of superconductivity we also need a Green's function which describes the breaking of a paired state. This is provided by the anomalous Green's function

$$F(x,t;x',t') = \langle \Psi_\downarrow(x,t)\Psi_\uparrow(x',t') \rangle , \tag{2.8}$$

which first "removes" from the system one electron of the Cooper pair at (x',t') and then the other, with opposite spin, at (x,t). Besides F and G, extra functions are introduced in order to include the operations on holes and to consider all possible spin combinations, for instance in the equal-spin triplet state. The BCS Hamiltonian can now be rewritten in terms of Green's functions [5], and the resulting equation has a similar form as the BdG equation (Eq.2.6), with the Green functions replacing the eigenfunctions [6]. This formalism allows important simplifications. In this case, like in any system, the fast oscillating components, which depend on $x - x'$, can be separated from the slower components, which depend on the center-of-mass position $(x' + x)/2$. As a result, since the fast oscillating part is canceled by the averaging, only the longer range features (longer than λ_F) remain. The second simplification applies to the scattering potential. In the dirty limit, instead of looking at the single impurities as for the BdG equation, we can consider an effective disorder potential. The outcome

of these (quasiclassical) approximations is the Usadel equation [7]

$$\hbar D\,[F\nabla^2 G - G\nabla^2 F] \;=\; -2i\Delta G - 2iEF, \tag{2.9}$$

where D is the electronic diffusion coefficient, Δ the superconducting gap and E the energy of the excitation respect to the Fermi level. The Usadel equation allows to describe real diffusive systems and can be applied to characterize the proximity effect (see Sec.2.2). In this case, however, because the formalism is built on the assumption that the two spin bands are equally populated, it fails in describing the superconductivity induced in a ferromagnet. It stays valid only in the limit of very small exchange energy, namely for weak ferromagnets.

2.1.3 Critical field in a superconductor

After discovering superconductivity, Kamerlingh Onnes was determined in exploiting the perfect conductance to build powerful superconducting magnets. Unfortunately he soon had to realize that there was a limit to the magnetic field a superconductor could sustain. We already discussed the Meissner-Ochsenfeld effect: a superconductor expels the magnetic field. But this is true up to a certain value, called the critical field B_c. The effect of the critical field divides the superconductors in two main categories: type-I and type-II (Fig.2.2). For Type-I superconductors there is one critical field which separates the superconducting state from the normal state. The critical field is temperature dependent and the typical behavior is shown in Fig.2.2a. For the type-II cases, two critical fields occur, B_{c1} and B_{c2} (see Fig.2.2b). Below B_{c1} the material is fully superconducting, above B_{c2} it is in the normal state. In the intermediate state the sample is still superconducting but the magnetic field penetrates in the form of filaments (or vortices). The vortices consist of normal regions through which there is quantized magnetic flux, a fluxoid of magnitude $\Phi_0 = \hbar/2e$. The normal cores are surrounded by circulating superconducting currents which screen the magnetic field outside the core. The direction of the circulating current is such that the generated magnetic field is parallel the external applied field. The radius of the core is equal to ξ_{GL}, while the decay length from the center of the core is given by the penetration depth λ. B_{c2} is basically defined by the maximum flux density sustainable by the superconductor, which corresponds to a spacing between the vortices of about ξ_{GL}. Abrikosov, by using the Ginzburg-Landau theory, could accurately describe the physics of vortices and could show that they arrange themselves in a periodic lattice [9], usually triangular. The prediction was confirmed experimentally with sev-

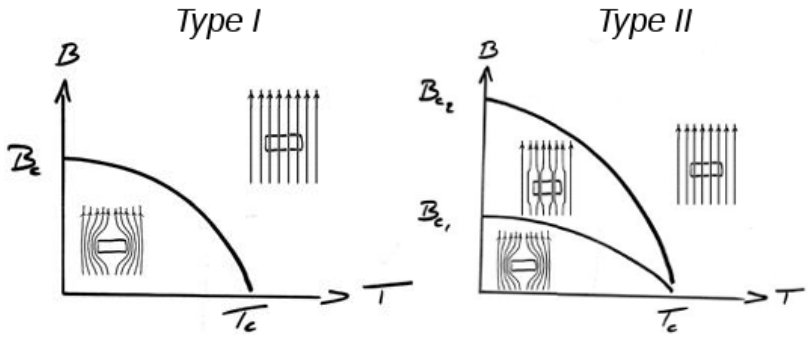

(a) (b)

Figure 2.2: Phase diagram B_c vs T for a type-I (a) and a type-II superconductor (b). Type-I superconductors have only one critical field (temperature dependent) which separates the superconducting from the normal phase. Type-II superconductors show two critical field values: below B_{c1} there is flux expulsion, above B_{c2} the material is in the normal state, in between B_{c1} and B_{c2} the material is still superconductor but there are normal regions (vortices) through which magnetic flux can penetrate. From Ref. [8].

eral imaging methods. The dynamics of the vortices can influence the current flowing through the superconductor. The field **B** of the fluxoids interacts with the transport current **I**, via the Lorentz force

$$\mathbf{F} = \mathbf{I} \times \mathbf{B}. \tag{2.10}$$

The force can move the vortices in the direction perpendicular to the current, with the normal cores now dissipating energy. Therefore the motion of vortices adds a finite resistance and is detrimental for applications. The dissipation can be avoided if the vortices are pinned to a certain position due to, for example, impurities (pinning centers). In general, according to the various conditions (current density, material, temperature, field strength) the lattice of vortices can be in the different states: we can have a pinned lattice, a more disordered but static glassy state, or moving vortices either in a coherent or disordered way. The contribution of vortex motion can be observed in the $R(B)$ transition curve. An example is shown in the schematic of Fig.2.3. The width of the transition (always larger for type-II superconductors) is due to the presence of vortices and a change in the vortex dynamics results in a change of the slope. From an experimental $R(B)$ curve there are different operational ways to define the upper critical field B_{c2}. As shown in Ref. [11, 12], for a weakly pinning material a good estimate is obtained by the intercept of the normal resistance value R_N and the fitting line of the linear part of the transition, which is the flux flow regime (see Fig.2.3).

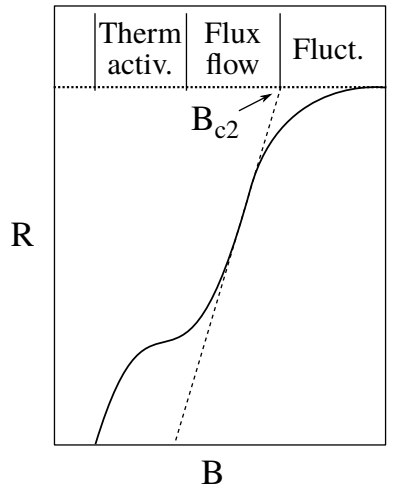

Figure 2.3: Schematic of a typical $R(B)$ transition curve for a type-II superconducting. The different vortex-flow regimes (thermal activation, flux flow and fluctuations) are indicated are indicated at the top. The arrow shows how the upper critical field B_{c2} value is typically determined, namely by the intercept of the fitting line of the linear part of the transition with the normal resistance value R_N. B_{c2} corresponds to the upper limit of the flux flow regime. From Ref. [10].

In the region below B_{c2} the material is still superconductor with a finite resistance due the flux flow, above B_{c2} there are fluctuations before the normal state is reached.

The dependence of the upper critical field H_{c2}[i] on the temperature has a universal behavior for all the superconductors. For a bulk superconductor (3D), close to the critical temperature T_c, the dependence is given by

$$H_{c2}(T) = \frac{\Phi_0}{2\pi\xi_{GL}^2(T)} = H_{c2}(0)\left(1 - \frac{T}{T_c}\right), \tag{2.11}$$

where $H_{c2}(0) = \Phi_0/2\pi\xi_{GL}^2(0)$ is the critical field at 0 K. For a thin film (2D, thickness $d \ll 2\xi_{GL}$), namely when the thickness is smaller than the coherence length, the behavior depends on whether the field is applied out-of-plane (perpendicular) or in-plane (parallel). In the first case the dependence is linear as in Eq.2.11, because in the direction perpendicular to field, i.e. along the plane, there is no confinement of the order parameter, as for a bulk sample. In the second case, it has a square-root

[i] Very often in the literature, when discussing about the critical field effects, the applied field H is considered rather than induction B. For this reason from now on we will use H_c as critical field.

dependence

$$H_{c2}(T) = H_{c2}(0)\sqrt{1-\frac{T}{T_c}}. \tag{2.12}$$

From the study of the phase diagram it is therefore possible to obtain information about the properties of the superconductor, in particular its coherence length, and the dimensionality. For for a 2D film

$$H_{c2\perp}(0) = \frac{\Phi_0}{2\pi\xi_{\mathrm{GL}}^2} \tag{2.13}$$

$$H_{c2\parallel}(0) = \frac{\sqrt{12}\,\Phi_0}{2\pi\xi_{\mathrm{GL}}d}, \tag{2.14}$$

where d is the layer thickness. In fact, when the field is applied parallel, a third critical field H_{c3} has to be taken into account. In general, when the applied field H approaches H_{c2} from above, the order parameter can nucleate at the edge of the sample before vortices are formed. The thickness of the superconducting sheet in this case is ξ (instead of 2ξ), which implies a higher critical field. Calculations show that in the dirty limit ($\ell < \xi_0$) the surface critical field H_{c3} is given by $H_{c3} = 1.69 \cdot H_{c2}$ [13]. For more details see Ref. [14].The analysis of the critical field dependence becomes particularly interesting in hybrid systems, where a superconductor is put next to a different material such as a normal metal or a ferromagnet in a bilayer or multi-layered structure. In the next section we will look at how the superconductivity is affected by the proximity with a non-superconducting material and how superconductivity is induced in a non-superconducting material.

2.2 Proximity effect

When a superconductor (S) is placed next to a normal metal (N), the superconducting order parameter Ψ does not vanish at the interface but penetrates the N layer. It decays within a certain range defined by the coherence length which, in the dirty limit, is given by

$$\xi_N = \sqrt{\frac{\hbar D_N}{k_B T}}, \tag{2.15}$$

where $\hbar$ is reduced Planck constant, D_N the diffusion coefficient of the normal metal, k_B the Boltzmann constant and T the temperature. A sketch of the behavior of Ψ at an S/N interface is shown in Fig.2.4. At low temperatures and for conventional met-

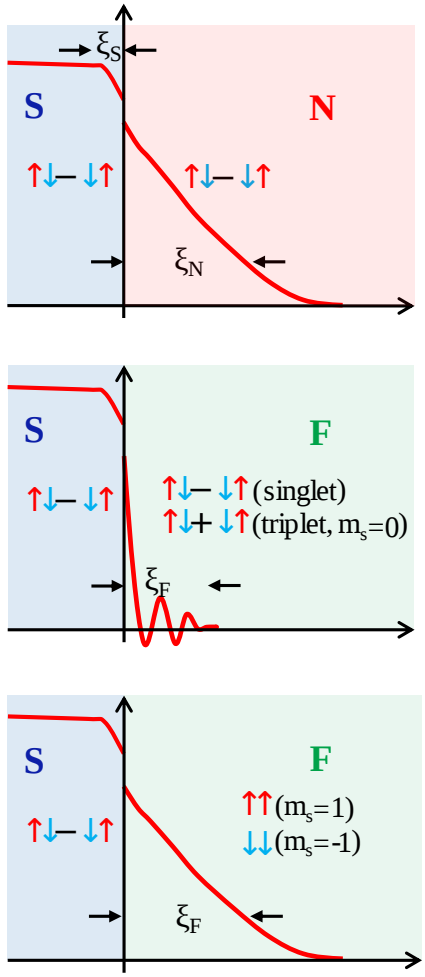

Figure 2.4: Schematic of the proximity effect which shows the behavior of the superconducting order parameter (red curve) in three cases: at the interface superconductor (S)/normal metal (N) (top panel), at interface superconductor (S)/ ferromagnet (F) (middle panel), at interface superconductor/ferromagnet when the equal-spin triplet component is generated (bottom panel). $\xi_{N,F}$ is the coherence length of either the N layer or the F layer.

als (e.g. copper), this length can be of the order of a micrometer. On the superconductor side, in the vicinity of the interface, the order parameter is depleted within a region equal to the (Ginzburg-Landau) coherence length of the superconductor $\xi_S(T)$ (equivalent to $\xi_{GL}(T)$ of Eq.2.5). The phenomenon of induced superconductivity on the normal metal is called proximity effect, while the reduction on the S side is known as inverse proximity effect. For simplicity the whole effect can be seen as the result of Cooper pairs leaking from the superconductor into the normal metal. However a more correct description of the actual mechanism is given by introducing the concept of Andreev reflection. An electron on the N side with energy ϵ lower than the gap Δ cannot be injected into the superconductor as a single quasiparticle, but has to form a Cooper pair. This is possible if the injection of the electron is accompanied by the simultaneous injection of a second electron from the valence band, with opposite spin (singlet pairing) and exactly opposite momentum and energy $-\epsilon$ (respect to E_F). On the N side, this is equivalent to the retro-reflection of a hole. The net effect is thus a charge transfer of $2e$ with no transfer of energy. Since the momentum of the reflected hole is exactly opposite to the incoming electron, it follows its original path. As long as electron and hole are phase coherent, the pair is indistinguishable from a Cooper pair, so that superconducting properties are induced in the normal metal even without the existence of an attractive pairing mechanism. When describing the proximity effect, thus, it would more appropriate to talk about induced "superconducting correlations" rather than induced Cooper pairs. However, for simplicity in this thesis we will often refer to the phenomenon as induced Cooper pairs, in line with the language typically used in literature. The coherence length, defined in Eq.2.15, basically measures the distance from the interface up to which the phases of the correlations stay coherent, when averaging over all energies below the gap. The interface transparency plays an important role in determining the strength of the proximity effect. A non-perfect quality of the interface and the band mismatch between the two materials, indeed, partially hinders the injection of Cooper pairs into N. This results in a discontinuity of the order parameter across the interface, as depicted in Fig.2.4.

2.2.1 Proximity effect in superconductor/ferromagnet hybrids

How does the proximity effect change if a ferromagnet is placed next to the superconductor, instead of a normal metal? As already introduced in Chap.1, the exchange energy E_{ex} of the ferromagnet strongly affects the proximity. On the one hand, because the two spin bands are not equally populated, the Andreev reflection is partially sup-

pressed (or completely in case of half-metals). On the other hand, E_{ex} strongly affects the induced superconducting correlations by forcing the spins to be parallel, therefore breaking the phase coherence between the injected electron and the reflected hole. For diffusive ferromagnets the characteristic penetration length of the order parameter is given by the coherence length ξ_{F} (Eq.1.1). For a standard ferromagnet this length is only a few nanometers. For a 100% spin-polarized material such as CrO_2, in which only one spin band in available at the Fermi level, the (singlet) Cooper pairs cannot be injected at all. The S/F interface is thus fully "reflective" and ξ_{F} is of the order of atomic distances.

The short range decay is not the only characteristic of the penetration of the order parameter in a ferromagnet: as can be seen from the middle panel of Fig.2.4, the function has an oscillatory behavior. This can be explained by considering the other superconducting components. Indeed, besides the singlet pairing, theoretically a Cooper pair can exists in three other states (triplet). The four possible states are

$$\begin{array}{lll} \textsc{Singlet} & \left\{ \begin{array}{ll} |\uparrow\downarrow - \downarrow\uparrow\rangle & m_{\mathrm{s}} = 0 \end{array} \right. \\ \textsc{Triplet} & \left\{ \begin{array}{ll} |\uparrow\uparrow\rangle & m_{\mathrm{s}} = +1 \\ |\uparrow\downarrow + \downarrow\uparrow\rangle & m_{\mathrm{s}} = 0 \\ |\downarrow\downarrow\rangle & m_{\mathrm{s}} = -1 \end{array} \right. , \end{array}$$

where m_{s} is the magnetic quantum number, which represents the projection of the total spin along the direction of quantization, defined by the exchange field. The oscillatory behavior is a mixture of the singlet with the $m_{\mathrm{s}} = 0$ triplet component. This can be seen as follows: in a ferromagnet the subbands for spin-up and spin-down are shifted by an amount $2E_{\mathrm{ex}}$. For this reason the two electrons forming the Cooper pair with opposite spin and opposite momentum ($+\mathbf{k}$, $-\mathbf{k}$), in order to adjust to the Fermi level in the ferromagnet, have to shift their momenta by an amount $\mathbf{Q}/2$. A schematic of the process is shown in Fig.2.5. So for spin-up we have $\mathbf{k}_{\uparrow} = \mathbf{k}+\mathbf{Q}/2$, for spin-down $\mathbf{k}_{\downarrow} = -\mathbf{k}+\mathbf{Q}/2$). As a result the Cooper pair acquires a nonzero center-of-mass momentum $\mathbf{Q}$. The amplitudes of the components $|\uparrow\downarrow\rangle$ and $|\downarrow\uparrow\rangle$ become modulated in space by a factor $\exp[\pm i(\mathbf{k}_{\uparrow} + \mathbf{k}_{\downarrow})\cdot\mathbf{R}]$ respectively. As a result [15] we have

$$|\uparrow\downarrow - \downarrow\uparrow\rangle \Rightarrow |\uparrow\downarrow\rangle\, e^{i\mathbf{Q}\cdot\mathbf{R}} - |\downarrow\uparrow\rangle\, e^{-i\mathbf{Q}\cdot\mathbf{R}} = |\uparrow\downarrow - \downarrow\uparrow\rangle \cos(\mathbf{Q}\cdot\mathbf{R}) + i\,|\uparrow\downarrow + \downarrow\uparrow\rangle \sin(\mathbf{Q}\cdot\mathbf{R}). \quad (2.16)$$

Thus the singlet component is mixed with the $m_{\mathrm{s}} = 0$ triplet component and the overall behavior is oscillating. The same mixing can result from a reflection for a spin polarized interface barrier. In this case the electrons acquire a spin dependent phase θ,

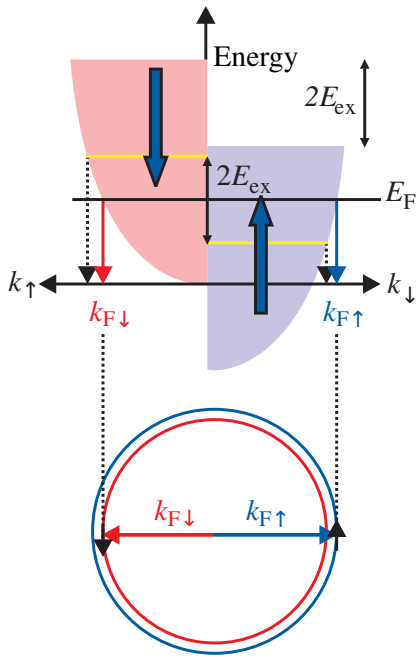

Figure 2.5: Depiction of the electronic structure for a ferromagnet. At an S/F interface, when the electrons pass from to S to F they have to adjust to the Fermi level E_F. Because the exchange energy shifts the two spin bands, $\mathbf{k}_\uparrow$ (blue) and $\mathbf{k}_\downarrow$ (red) shift accordingly. As a result, the Cooper pair acquires a finite center-of-mass momentum. From Ref. [15].

which modulates the amplitude by a factor $\exp[\pm i\theta]$. This is the only possible mechanism for spin-mixing in presence of half-metals, where the injection is (almost) completely forbidden for the spin of the minority band.

The fact that the superconducting order parameter has an oscillating dependence on the distance from the S/F interface has an interesting implication: the possibility of having a π-Josephson junction. A Josephson junction is a structure made by two superconductors separated by a non-superconducting material. If the length of the spacer, in our case a ferromagnet, is within two times the coherence length ξ_F, a supercurrent can be injected from on side of the junction to the other, across the ferromagnetic layer. The two superconductors are then coupled and quantum coherent effects are observed. If the superconducting order parameter oscillates from positive to negative values along the F layer, by varying the length of the spacer, namely the position of the second F/S interface, it is possible to switch from a positive (0-junction) to a negative current direction (π-junction). This results in an oscillating behavior of the critical current which can be explored either by varying the length of the F layer [16,17] or the temperature [18,19]. The possibility of switching between the two states, 0- and π-junction, is interesting for the development of electronic devices. Experimental evidence of such switching could be shown for extremely diluted ferromagnets, such as CuNi [18], PdNi [16], but also for Ni [17,20], $Ni_{80}Fe_{20}$(Py) and Co [20]. However, a big limitation for the development of applications is the short range of the proximity effect in S/F systems. More details about the working principle and the properties of Josephson junctions will be discussed in Sec.2.3.1.

2.2.2 Long-range proximity effect

The possible scenarios offered by S/F systems are not limited to a short range, oscillating proximity. A long-range proximity effect can be induced and, surprisingly, Cooper pairs can be injected into a ferromagnet and exist for distances up to several hundreds nanometers, as for a normal metal. In order to overcome the pair-breaking mechanism of the exchange energy, the standard singlet Cooper pairs have to be converted into the triplet state $|\uparrow\uparrow\rangle$ (or $|\downarrow\downarrow\rangle$) thus with $m_s = 1$ (or -1), in which the spins are aligned parallel. This is possible even for conventional superconductors characterized by singlet coupling: if a certain degree of magnetic non-collinearity is provided at the S/F interface the triplet $m_s = 0$ component, introduced in the previous section, can be converted into the spin-parallel one. Indeed, the $m_s = 0$ component is not rotationally invariant. Therefore, if the magnetization vector, so the direction of the quantization,

changes direction along the path crossed by the Cooper pairs, this component is rotated in the spin space and converted as shown in Fig.2.6. For instance, if at the S/F

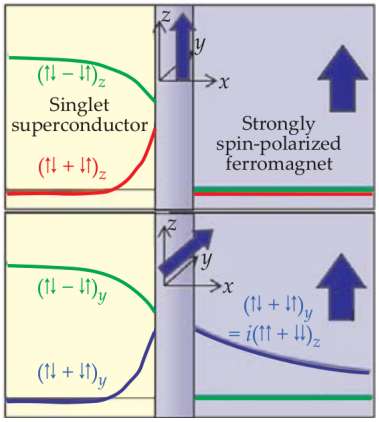

Figure 2.6: Sketch which shows the mechanism of singlet-to-triplet conversion at an S/F interface. If the at interface there are misaligned magnetic moments, the $m_s = 0$ triplet component is rotated in the spin space and converted into the spin-parallel triplet component. From Ref. [15].

interface the magnetization is aligned along the y-axis and, within a length ξ_F, it is rotated to the z-axis, the component with projection $m_s = 0$ along y will have a nonzero projection along z. The result is the conversion $|\uparrow\downarrow + \downarrow\uparrow\rangle_y \Rightarrow |\uparrow\uparrow + \downarrow\downarrow\rangle_z$. The conversion efficiency is maximized when the angle between the magnetization directions is 90 degrees. The amount of polarization of the the ferromagnet defines the relative amplitude of the two components $\uparrow\uparrow$ and $\downarrow\downarrow$. In the case of the half-metals, one of the two is completely suppressed. In most of the cases, the main limiting factor for the long-range proximity effect is the spin diffusion length. The spin diffusion length measures the characteristic distance traveled by the electron inside the ferromagnet before the occurrence of a scattering event which flips the spin. Once the spin of one of the two electrons is flipped, the triplet alignment is lost and the Cooper pairing is broken by the exchange interaction. For Co, the polarization is about 42% [21] and the spin diffusion length is expected to be 60 nm [22, 23]. For CrO_2, 100% spin-polarized, the spin flipping is not a problem and the limiting factor for the coherence length, as for a normal metal, is the diffusion coefficient D_F, via the relation:

$$\xi_F^T = \sqrt{\frac{\hbar D_F}{k_B T}}, \tag{2.17}$$

As already mentioned in Sec.1.3, in order to be compatible with a long range in a diffusive ferromagnet, the superconducting triplet coupling has to be spin-parallel, s-wave and odd-frequency. In Sec.1.3 an intuitive picture to understand the meaning of the odd-frequency was given. A more rigorous explanation involves the use of the Gor'kov formalism. A detailed description and a review about odd-frequency superconductivity can be found in Ref. [24].

2.3 Superconducting devices

By combining superconducting with non-magnetic layers we can build superconducting devices, in which the proximity effect plays a crucial role in determining the properties. The two systems of main interest for our research are Josephson junctions (JJs) and triplet spin valves (TSVs). In our work we fabricate these devices in order to provide an experimental evidence for the (long-range) proximity effect. In a JJ, if superconducting coupling is observed across the ferromagnetic spacer, it means that the intermediate layer has been fully proximized and that the supercurrent could survive from one side to the other. In a TSV, as will be explained in Sec.2.3.2, by looking at the variations of the properties of the superconducting layer, it is possible to indirectly infer proximity with the adjacent layers. In a broader perspective, such superconducting devices are interesting for their peculiar properties and their applications. A JJ, for example, because of its quantum properties is already used as sensitive voltage probe (SQUID) and is promising as a building block for superconducting electronics or quantum computers. A TSV could be in principle used for generating spin-polarized supercurrents, in combination with more complex electric circuits, or as field sensors. However, the development of such applications is not the goal of this work. JJs and TSVs, the details of which will be described in the following sections, are here mainly used as tools to investigate the proximity effect.

2.3.1 Josephson junctions

The Josephson effect, originally demonstrated for an insulating spacer (I) in an S/I/S device, is an example of quantum behavior which manifests itself at the macroscopic scale. The effect, proposed by Josephson in 1962, allows the cotunneling of the two electrons forming a Cooper pair from one side of the junction to the other, through the insulating layer. When this happens, the S layers are coupled and the conduction

properties of the junction depend only on the macroscopic properties of the superconductors, in particular on the phase difference between the superconducting condensate of the S layers, $\phi(t) = \vartheta_1(t) - \vartheta_2(t)$. The equations for voltage and current as function of time are

$$V(t) = \frac{\hbar}{2e}\frac{\partial \phi}{\partial t} \tag{2.18}$$

$$I_S(t) = I_c \sin(\phi(t)), \tag{2.19}$$

where $\hbar$ is the Planck constant, e the charge of the electron and I_c the critical current of the junction at zero field. From Eq.2.19 we can see that, up to the critical value I_c, it is possible to have a current flowing even with zero applied voltage (if $\phi(t) \neq 0$). This peculiar property is illustrated in Fig.2.7 which shows a typical $I-V$ characteristic for a Josephson junction. The same behavior is observed when the insulating gap is re-

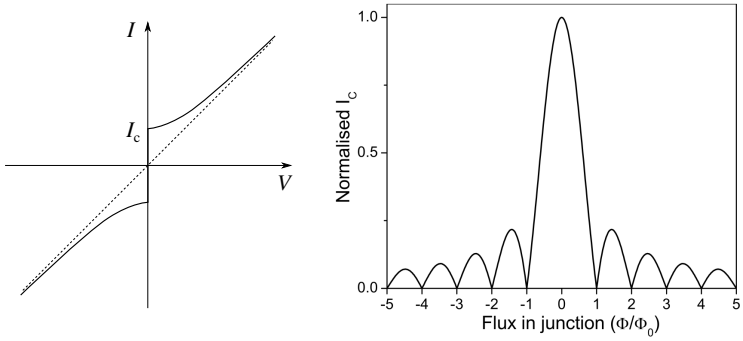

Figure 2.7: Left panel: typical $I-V$ characteristic of a Josephson junction (full line)(from Ref. [1]). The dashed line shows the linear slope for a standard ohmic dependence. Right panel: theoretical Fraunhofer pattern for a Josephson junction (from Ref. [25]).

placed by either a normal metal or a ferromagnet, in an S/N/S or S/F/S junction. In this case the transfer of Cooper pairs does not happen via tunneling but via Andreev reflection, which proximizes the intermediate layer. In order to have Josephson coupling the spacer length has to be smaller than two times the coherence length of the proximized layer. The quantum behavior unfolds even more explicitly when a magnetic field is applied perpendicular to the current direction. When a field is applied, the vector potential interacts with the supercurrent adding an extra phase difference, which is proportional to the magnitude of the field. By increasing the field we can observe an oscillating behavior of the critical current, due to the periodicity of the phase, superimposed on the decay due to the orbital breaking effect. The result is the char-

acteristic behavior shown in Fig.2.7, known as the Fraunhofer pattern, because of the similarity with the pattern observed in optical diffraction. The period of the oscillations is equal to $\Delta B = \Phi_0 \cdot A$, where Φ_0 is the quantum magnetic flux and A is the area of the junction penetrated by the magnetic field (flux).

In order to have a long-range proximity effect in an S/F/S junction the singlet superconductivity of the S layers has to be converted into triplet and for that to happen, as we have already discussed, it is essential to provide misaligned magnetic moments at the S/F interface. Via the same mechanism the triplet supercurrent in the F layer needs to be converted back into singlet before being injected into the second S lead. In this case the junction can be better described by a multilayer S/F'/F/F"/S, where F' and F" represent the region of the ferromagnet where the magnetic moments are misaligned with respect to F. In most of the experiments F' and F" are separate magnetic layers, the magnetization of which can be controlled independently by F. As shown in Fig.2.8, the relative orientation of the magnetization of F', F and F" is crucial to determine the amplitude of the critical current of the junction. The bottom graph of Fig.2.8 is the result of a computation by Houzet and Buzdin [26], where the normalized critical currents I_c are plotted as a function of the normalized thickness of the F' layer (F" has the same thickness). If the magnetizations of F' and F are kept fixed with a relative angle Φ_L at the optimum value $\pi/2$, the I_c value strongly depends on the angle between F and F", called ϕ_R. The maximum occurs for $\phi_R = -\pi/2$, namely with F' and F" magnetized antiparallel. If magnetizations are parallel, or in general with $0 < \phi_R \leqslant \pi/2$, a π-junction behavior is expected. The importance of controlling both interfaces is one of the factors which makes it experimentally challenging to fabricate a "working" triplet Josephson junction. An alternative, even if less direct, way of probing the long-range proximity effect can be achieved, as we will see in the following section, by studying a simpler device, the triplet spin valve.

2.3.2 Triplet spin valve

A superconducting spin valve, in general, is a multilayer structure made by one superconductor (S) and two ferromagnets (F_1 and F_2), where the superconducting properties of the S layer depend on the relative magnetization orientation of the F layers. In conventional superconducting spin valves the structure is $F_1/S/F_2$, with the superconductor (not thicker than a few times ξ_s) in the middle. These devices have been extensively studied both theoretically [27, 28] and experimentally [29–31] by measuring the difference in T_c between parallel and antiparallel alignment of F_1 and F_2. This geometry can be used to investigate the triplet superconductivity [32], on condition

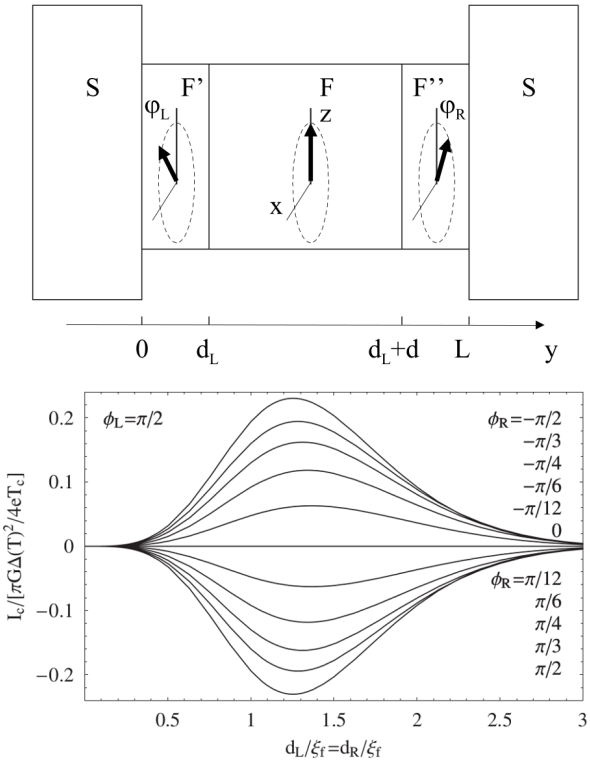

Figure 2.8: .Top: geometry of an S/F'/F/F"/S junction. The arrows indicate noncollinear orientations of the magnetizations in each layer with thicknesses d_L, d, and d_R, respectively. Bottom: normalized critical current I_c induced in a an S/F'/F/F"/S junction, for varying length of F' and F" layers, at $d_L = d_R \approx \xi_F \ll d \ll \xi_0$, and for different orientations of the magnetization of F" (angle Φ_R). Φ_L is fixed at $\pi/2$. From Ref. [26].

that magnetic inhomogeneities are provided, however it is not the most suitable one for this purpose. The generation of triplets can be more easily controlled and studied in a multilayer structure $S/F_1/F_2$ [33], the so-called superconducting triplet spin valve (TSV) [34]. In this case F_1 is called mixer layer and F_2 drainage layer. A TSV can be thought of as half of a Josephson junction, so with only one interface to control. If we refer to the previous section, the correspondence is F'→F_1 and F→F_2. In a TSV the generation of triplet Cooper pairs is inferred by the change of the superconducting properties of the proximized multilayer. The superconducting order parameter of a proximized superconductor, constant in the bulk, is depleted in a region close to the interface (inverse proximity effect) with the characteristic length scale of the depletion given by the coherence length ξ_S. So, if the thickness of the S layer does not exceed a few times ξ_S, the superconducting properties of the layer are affected by the proximity, this because the macroscopic critical temperature is proportional to the average of the amplitude to the order parameter in the whole layer. The stronger the proximity, the larger the effect on the superconducting side. This is the basis of the working principle of a TSV, which is shown in Fig.2.9. We have already seen that, in order to

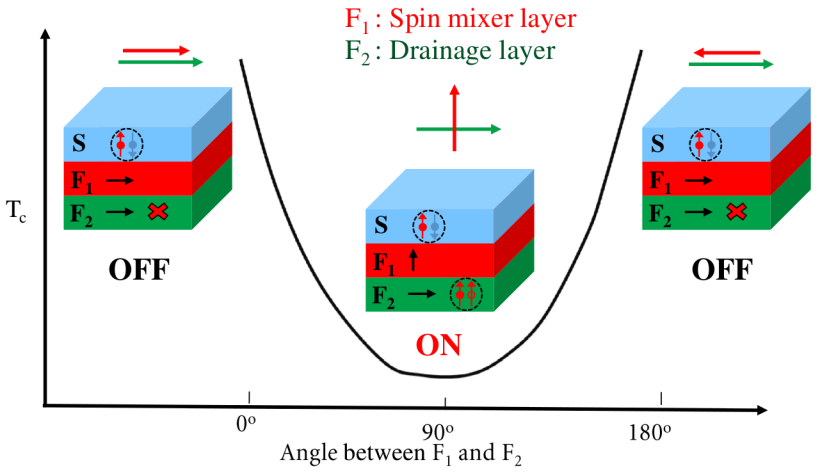

Figure 2.9: Working principle of a superconducting triplet spin valve (TSV). If the magnetizations of F_1 and F_2 are parallel (or antiparallel) there is no generation and the valve is "off". If they are misaligned, triplet Cooper pairs are generated and injected into the F_2 layer, with a consequent stronger depletion of the order parameter on the S side: the valve is "on". This results in a suppression of the critical temperature T_c. Note that the misalignment can be either in-plane or out-of-plane.

have singlet-to-triplet conversion, we need misaligned magnetic moments so that the $m_s = 0$ triplet component is rotated into the $m_s = 1$ component, with equal spin. So if

the magnetizations of F_1 and F_2 are aligned parallel (or antiparallel) there is no generation and the valve is "off". If they are misaligned (either in-plane or out-of-plane) the TSV is "on": triplet Cooper pairs are generated and injected into the F_2 layer, with a consequently stronger depletion of the order parameter on the S side. This results in a suppression of the critical temperature T_c, with the minimum expected when the two magnetizations are perpendicular to each other. The non-monotonic dependence of T_c on the relative angle between the magnetization vectors is a peculiar signature of TSVs. For a standard (singlet) spin valve, in the same geometry but with no triplet induction, we would expect a monotonic decrease from the parallel to the antiparallel configuration, due to the different pair-breaking effective exchange field, lower in the latter case [33]. It is important to stress that there is an optimal value for the thickness of the mixer layer F_1. The length scale for it is set by the coherence length of F_1, ξ_{F_1}: if the F_1 layer is much thicker, the induced (short range) Cooper pairs vanish within the layer without being converted; if F_1 is too thin the spin mixing mechanism which generates the $m_s = 0$ component is not efficient enough. For this reason the dependence of the TSV effect on the thickness of the mixer layer is expected to be non-monotonic with a maximum around the optimal value. T_c is not the only interesting quantity to look at for a TSV. In fact, the upper critical field H_{c2} can provide useful insight into the study of the triplet channel in such devices. This is particularly true in the experiments where a magnetic field is applied in order to vary the relative orientation of F_1 and F_2. In this case, the variation of T_c could be the result of the change of critical field which, as pointed out in 2.1.3, depends on the orientation of the applied field.

2.4 Ferromagnetism

In the previous sections we have already discussed the role of the exchange energy in the pair-breaking and the importance of magnetic inhomogeneities for the generation of triplet superconductivity. In this section we want to provide further insight into the ferromagnetism in general. A material which shows an intrinsic magnetic moment, with no applied field, is a ferromagnet. The macroscopic effect is the result of the additive contributions of the small dipole magnetic moments at the microscopic level. These dipoles are mainly due to the orbital and the spin moments of the electrons, with the spin giving the major contribution. The magnetic moment of an electron is equal to a Bohr magnetron $\mu_B = e\hbar/2m_e$=9.27 J/T. In general, because of the Pauli principle, every completed energy state is occupied by two electrons with antiparallel spins, so with resultant zero magnetic moment. The strong magnetic effects originate

from a small fraction of unpaired electrons.

There are two models to describe ferromagnetism: in the first model, used e.g. for magnetic insulators and $4f$ metals, the contributing moments are localized, in the second one, which describes magnetic $3d$ transition metals, they are itinerant. Here we will briefly present the latter model, also called band model, which describes the most common ferromagnets, such as Co, Fe and Ni [35]. In the transition (ferromagnetic) metals, the outer occupied (or semi-occupied) bands are $4s$ and $3d$, with the spin-up $3d_\uparrow$ and spin-down $3d_\downarrow$ sub-bands shifted due to the exchange energy E_{ex} (see Fig.2.10, left panel). As a consequence $3d_\uparrow$ and $3d_\downarrow$ are not equally occupied and this results in a net magnetic moment. In the case of Ni, for example, $3d_\uparrow$ is fully occupied by 5 electrons, while the $3d_\downarrow$ is partially empty, with about 0.6 holes due to 0.6 electrons transferred to the $4s$ band. As a result Ni has a magnetic moment of about 0.6 μ_{B} per atom. For comparison, the moments of Fe and Co are 2.2 and 1.7 μ_{B}, respectively. The origin of the exchange interaction is purely quantum mechanical and

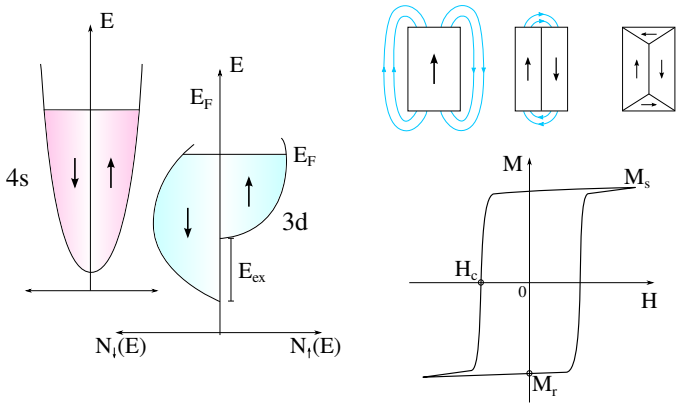

Figure 2.10: Left: schematic of the band structure of an itinerant ferromagnet close to the Fermi level (adapted from Ref. [36]). Top right: sketch of a confined structure with different magnetic configurations: the presence of magnetic domains minimizes the stray field. Bottom right: typical hysteresis loop $M(H)$ for a ferromagnet.

a direct consequence of the Pauli exclusion principle. It exists only between particles with parallel spin: since they cannot exist in the same state, the expectation value of their distance is increased respect to the antiparallel state. The increase of the distance reduces the overlap of neighbor orbitals with a consequent decrease of the potential energy (lower Coulomb repulsion). For this reason, it can be more favorable for the

spin to be aligned parallel. The result is then a shift of the spin sub-bands. It can be shown that the condition for that to happen is given by the Stoner criterion

$$I \cdot \widetilde{D}(E_{\mathrm{F}}) > 1, \tag{2.20}$$

with I the exchange integral and $\widetilde{D}(E_{\mathrm{F}}) = (V/2N) \cdot D(E_{\mathrm{F}})$, where V is the volume and $D(E_{\mathrm{F}})$ the density of states at the Fermi level. I is connected to the exchange energy E_{ex} via the relation $E_{\mathrm{ex}} = I(n_{\uparrow} - n_{\downarrow})/N$, where $n_{\uparrow(\downarrow)}$ is the number of electrons with spin-up (down) and N is the total number of electrons $n_{\uparrow} + n_{\downarrow}$. Typical exchange energy values are of the order of a few eV, three order of magnitude stronger than the superconducting coupling. If the thermal energy exceeds the exchange interaction, the ordered pairing is lost and the magnetic moments are randomized. The threshold temperature is given by the Curie temperature T_{C}.

The exchange energy determines the occurrence of magnetic order, but does not exclusively control the homogeneity of the magnetic state of a finite sample. In most of the cases, the magnetization of a ferromagnetic sample is not homogeneously oriented in one direction but subdivided in smaller domains. The rotation of the magnetization from one domain to the other happens within a domain wall. The final magnetic configuration is the one which minimizes the total free energy density, which in the static case is given by [37]

$$\begin{aligned} E_{\mathrm{tot}} = & \underbrace{A\,(\nabla \mathbf{m})^2}_{\text{exchange energy}} + \underbrace{\varepsilon_{\mathrm{an}}}_{\text{crystalline anisotropy}} + \underbrace{\frac{1}{2}\mu_0 \mathbf{M}\cdot\mathbf{H}\mathrm{d}}_{\text{demagnetizing energy}} - \underbrace{\mu_0 \mathbf{M}\cdot\mathbf{H}_{\mathrm{a}}}_{\text{Zeeman energy}} \\ & - \underbrace{\boldsymbol{\sigma}_{\mathrm{ex}}\cdot\epsilon^0}_{\text{external stress}} + \underbrace{\frac{1}{2}(\mathbf{p}_e - \epsilon^0)\cdot\bar{\bar{c}}\cdot(\mathbf{p}_e - \epsilon^0)}_{\text{magnetostriction energy}}, \end{aligned} \tag{2.21}$$

where A is the exchange stiffness constant (the first term is E_{ex}), $\mathbf{m}$ is the magnetization $\mathbf{M}$ normalized by the saturation magnetization M_{s}, $\mathbf{H}_{\mathrm{d}}$ and $\mathbf{H}_{\mathrm{a}}$ are the demagnetizing and the applied field, respectively; the second term is the energy term connected to the anisotropy of the crystallographic structure, which makes certain directions more energetically favorable; σ_{ex} is the external stress tensor, ϵ^0 the strain (namely the change in length divided by the total length), $\mathbf{p}_e$ the deviation from the initial non-magnetic state and $\bar{\bar{c}}$ the tensor of elastic constants. If there is no applied field, no magnetocrystalline anisotropy and no stress from external factors, the configuration is uniquely determined by the competing exchange and demagnetizing energy, also called shape anisotropy. If a sample is uniformly magnetized, the exchange

term is minimized (the gradient of **m** is zero) but the demagnetizing field $\mathbf{H}_d$, namely the stray field generated by M, is maximum. The exchange interaction is on atomic scales and short range while the demagnetizing energy derives from dipole fields and is dominant at larger scales. Thus, small samples (typically below micron size) are single domain while larger samples show a multi-domain configuration, which minimizes the stray field (see Fig.2.10 (right top)). In this case the ratio between domain size and domain wall width is determined by the ratio between the two energy terms. The shape of the sample strongly influences the demagnetizing field and therefore the domain configuration. In a thin film, for instance, the magnetization typically lies in-plane, so that the stray field is minimized. The orientation of the domains can be influence by other anisotropies, such as the crystalline anisotropy: when a crystallographic structure is present, aligning the magnetic moments along a particular direction of the lattice can be energetically favorable than along others. This has to do with the spin-orbit interaction of the electrons. The preferred directions can be one, or more, according to the type of crystalline anisotropy. The last two energy terms of Eq.2.21 are related to the deformation of the lattice - due to either external mechanical stress, or to an applied magnetic field - which causes displacement of the atoms of the crystal with a consequent modification of the overlap of the neighbor orbitals. These terms are usually negligible in conventional systems. The combination of all the anisotropies determines the "easy axis" of the sample, namely the energetically favorable direction(s) of spontaneous magnetization. A "hard axis", a direction of maximum energy and unfavorable, can also be present. When a magnetic field is applied, in order to minimize the Zeeman energy, the magnetic moments are rotated and aligned parallel to the applied field. The field above which all the (possible) moments are rotated is called saturation field H_{sat}. In this state the samples has the maximum magnetization M_s. If, after the first magnetizing procedure, the field is swept back a forth between $H > H_{sat}$ and $H < -H_{sat}$, the magnetization shows a characteristic hysteretic behavior (see Fig.2.10,right bottom). The width of the loop, defined by the field at which the magnetization changes its sign (i.e. the coercive field), says how difficult is to magnetize the ferromagnet: materials with a low coercive field are called "soft" ferromagnets, the ones with high coercive field "hard" ferromagnets. A single domain configuration will have a sharp transition, namely a rectangular hysteresis loop, while in a multi-domain ferromagnet the saturation happens gradually with different slopes depending on the the way the domains are rotated.

2.4.1 Ferromagnetism in CrO_2

CrO_2, as we have already discussed, is an interesting material because of its half-metallicity. In the previous section we saw that for the most common materials the ferromagnetism is due to the contribution of itinerant electrons of the valence band, while in other cases it is the result of more localized moments. CrO_2, in this respect, is a peculiar material. A band model can properly describe the behavior of the conduction electrons but fails to explain other experimental observations, such as the particular paramagnetic behavior above the Curie temperature T_C and the large temperature dependence of the resistivity (from over 220 $\mu\Omega$cm [38] close to T_C, to a few $\mu\Omega$cm at low temperatures). Both these behaviors are more consistent with a model of localized moments. Such a model, however, would lead to an Mott insulating-like and antiferromagnetic ground state [39], because of the strong correlations [40]. A

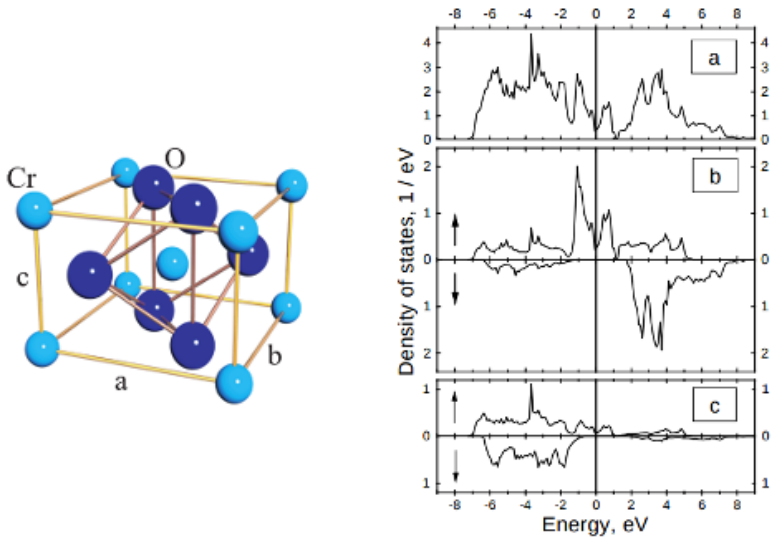

Figure 2.11: Left: rutile structure of CrO_2, with every Cr atom surrounded by 6 atoms in an octahedron. From Ref. [41]. Right: total density of states per formula unit and for both spins (a) and partial Cr $3d$ (b) and O $2p$ (c) density of states of CrO_2. From Ref. [39].

correct description, instead, is provided by a hybrid model which involves both itinerant and localized moments [39, 42]. CrO_2 has a rutile crystal symmetry (as TiO_2, RuO_2, VO_2 and MnO_2) with two Cr atoms in positions $[0,0,0]$ and $\left[\frac{1}{2},\frac{1}{2},\frac{1}{2}\right]$ and 4 O atoms at $[u,u,0]$, $[1-u,1-u,0]$, $\left[\frac{1}{2}+u,\frac{1}{2}-u,\frac{1}{2}\right]$ and $\left[\frac{1}{2}-u,\frac{1}{2}+u,\frac{1}{2}\right]$, with u about 0.3 [43]. These positions are such that every Cr atom is surrounded by 6 O atoms

forming an octahedron (see Fig.2.11). The lattice parameters are $a = b$ =4.419 Å and c =2.912 Å [43]. Cr is in a 4+ state with two unpaired electrons in the $3d$ band, O is in a 2- state. According to the model, one of the two electrons of Cr is localized and forms a narrow band below E_F (1 eV below), while the other hybridizes with the $2p$ bands, at the Fermi level. A plot of the density of state for CrO_2 and Cr and O separately, is shown in Fig.2.11(right). The metallicity of CrO_2 is due to a self-doping process: the most energetically favorable state is with some of the $2p$ electrons of O occupying the empty $3d$ bands of Cr. These electrons leave holes in the $2p$ bands at E_F, which are responsible for the conduction and have little correlation effects.

BIBLIOGRAPHY

[1] J. Annett. *Superconductivity, superfluids and condensates.* Oxford University Press (2003).

[2] V. L. Ginzburg and L. D. Landau. To the theory of superconductivity. *Zh. Eksp. Teor. Fiz.* **10**, 1064 (1950).

[3] L. P. Gor'kov. Microscopic derivation of the Ginzburg-Landau equations in the theory of superconductivity. *J. Exp. Theor. Phys.* **9**, 1364 (1959).

[4] N. N. Bogoliubov. A new method in the theory of superconductivity .1. *J. Exp. Theor. Phys.* **7**, 41 (1958).

[5] L. P. Gor'kov. On the energy spectrum of superconductors. *J. Exp. Theor. Phys.* **7**, 505 (1958).

[6] M. G. Flokstra. *Proximity effects in superconducting spin-valve structures.* Ph.D. thesis Leiden University (2010).

[7] K. D. Usadel. Generalized diffusion equation for superconducting alloys. *Phys. Rev. Lett.* **25**, 507 (1970).

[8] F. Bouquet and J. Bobroff. http://www.supraconductivite.fr.

[9] A. A. Abrikosov. The magnetic properties of superconducting alloys. *J. Phys. Chem. Solids* **2**, 199 (1957).

[10] J. M. E. Geers. *Superconductivity in thin films and multilayers. Vortex behavior and the interaction with magnetism.* Ph.D. thesis Leiden University (1999).

[11] P. Berghuis, A. L. F. van der Slot, and P. H. Kes. Dislocation-mediated vortex-lattice melting in thin-films of α-Nb_3Ge. *Phys. Rev. Lett.* **65**, 2583 (1990).

[12] P. Berghuis and P. H. Kes. Two-dimensional collective pinning and vortex-lattice melting in a-$Nb_{1-x}Ge_x$ films. *Phys. Rev. B* **47**, 262 (1993).

[13] D. Saint-James and P. G. de Gennes. Onset of superconductivity in decreasing fields. *Phys. Lett.* **7**, 306 (1963).

[14] V. V. Schmidt. *The physics of superconductors.* Springer (1997).

[15] M. Eschrig. Spin-polarized supercurrents for spintronics. *Phys. Today* **64**, 43 (2011).

[16] T. Kontos, M. Aprili, J. Lesueur, F. Genet, B. Stephanidis, and R. Boursier. Josephson junction through a thin ferromagnetic layer: negative coupling. *Phys. Rev. Lett.* **89**, 137007 (2002).

[17] Y. Blum, A. Tsukernik, M. Karpovski, and A. Palevski. Oscillations of the superconducting critical current in Nb-Cu-Ni-Cu-Nb junctions. *Phys. Rev. Lett.* **89**, 187004 (2002).

[18] V. V. Ryazanov, V. A. Oboznov, A. Y. Rusanov, A. V. Veretennikov, A. A. Golubov, and J. Aarts. Coupling of two superconductors through a ferromagnet: evidence for a π junction. *Phys. Rev. Lett.* **86**, 2427 (2001).

[19] V. A. Oboznov, V. V. Bol'ginov, A. K. Feofanov, V. V. Ryazanov, and A. I. Buzdin. Thickness dependence of the Josephson ground states of superconductor-ferromagnet-superconductor junctions. *Phys. Rev. Lett.* **96**, 197003 (2006).

[20] J. W. A. Robinson, S. Piano, G. Burnell, C. Bell, and M. G. Blamire. Critical current oscillations in strong ferromagnetic π junctions. *Phys. Rev. Lett.* **97**, 177003 (2006).

[21] R. J. Soulen, J. M. Byers, M. S. Osofsky, B. Nadgorny, T. Ambrose, S. F. Cheng, P. R. Broussard, C. T. Tanaka, J. Nowak, J. S. Moodera, A. Barry, and J. M. D. Coey. Measuring the spin polarization of a metal with a superconducting point contact. *Science* **282**, 85 (1998).

[22] L. Piraux, S. Dubois, A. Fert, and L. Belliard. The temperature dependence of the perpendicular giant magnetoresistance in Co/Cu multilayered nanowires. *EPJ B* **4**, 413 (1998).

[23] J. Bass and W. P. Pratt, Jr. Spin-diffusion lengths in metals and alloys, and spin-flipping at metal/metal interfaces: an experimentalist's critical review. *J. Phys. Condens. Matter* **19**, 183201 (2007).

[24] F. S. Bergeret, A. F. Volkov, and K. B. Efetov. Odd triplet superconductivity and related phenomena in superconductor-ferromagnet structures. *Rev. Mod. Phys.* **77**, 1321 (2005).

[25] C. Bell. *Nanoscale Josephson devices.* Ph.D. thesis St. John's College Cambridge (2003).

[26] M. Houzet and A. I. Buzdin. Long range triplet Josephson effect through a ferromagnetic trilayer. *Phys. Rev. B* **76**, 060504 (2007).

[27] L. R. Tagirov. Low-field superconducting spin switch based on a superconductor/ferromagnet multilayer. *Phys. Rev. Lett.* **83**, 2058 (1999).

[28] A. I. Buzdin, A. V. Vedyayev, and N. V. Ryzhanova. Spin-orientation-dependent superconductivity in F/S/F structures. *EPL* **48**, 686 (1999).

[29] J. Y. Gu, C. Y. You, J. S. Jiang, J. Pearson, Y. B. Bazaliy, and S. D. Bader. Magnetization-orientation dependence of the superconducting transition temperature in the ferromagnet-superconductor-ferromagnet system: CuNi/Nb/CuNi. *Phys. Rev. Lett.* **89**, 267001 (2002).

[30] A. Potenza and C. H. Marrows. Superconductor-ferromagnet CuNi/Nb/CuNi trilayers as superconducting spin-valve core structures. *Phys. Rev. B* **71**, 180503 (2005).

[31] I. C. Moraru, W. P. Pratt, Jr., and N. O. Birge. Observation of standard spin-switch effects in ferromagnet/superconductor/ferromagnet trilayers with a strong ferromagnet. *Phys. Rev. B* **74**, 220507 (2006).

[32] N. Banerjee, C. B. Smiet, R. G. J. Smits, A. Ozaeta, F. S. Bergeret, M. G. Blamire, and J. W. A. Robinson. Evidence for spin selectivity of triplet pairs in superconducting spin valves. *Nat. Commun.* **5**, 3048 (2014).

[33] S. Oh, D. Youm, and M. R. Beasley. A superconductive magnetoresistive memory element using controlled exchange interaction. *Appl. Phys. Lett.* **71**, 2376 (1997).

[34] Y. V. Fominov, A. A. Golubov, T. Y. Karminskaya, M. Y. Kupriyanov, R. G. Deminov, and L. R. Tagirov. Superconducting triplet spin valve. *J. Exp. Theor. Phys.* **91**, 308 (2010).

[35] C. Kittel. *Introduction to solid state physics.* John Wiley & Sons, Inc. 8^{th} edition (2005).

[36] M. Johnson. Spintronics. *J. Phys. Chem. B* **109**, 14278 (2005).

[37] A. Hubert and R. Schafer. *Magnetic domains.* Springer (1998).

[38] K. Suzuki and P. M. Tedrow. Resistivity and magnetotransport in CrO_2 films. *Phys. Rev. B* **58**, 11597 (1998).

[39] M. A. Korotin, V. I. Anisimov, D. I. Khomskii, and G. A. Sawatzky. CrO_2: a self-doped double exchange ferromagnet. *Phys. Rev. Lett.* **80**, 4305 (1998).

[40] C. F. Chang, D. J. Huang, A. Tanaka, G. Y. Guo, S. C. Chung, S. T. Kao, S. G. Shyu, and C. T. Chen. Electronic structure of CrO_2 studied by magnetic circular dichroism in resonant photoemission. *Phys. Rev. B* **71**, 052407 (2005).

[41] R. S. Keizer. *Singlet and triplet supercurrents in disordered mesoscopic systems.* Ph.D. thesis Delft Technical University (2007).

[42] D. J. Huang, L. H. Tjeng, J. Chen, C. F. Chang, W. P. Wu, S. C. Chung, A. Tanaka, G. Y. Guo, H. J. Lin, S. G. Shyu, C. C. Wu, and C. T. Chen. Anomalous spin polarization and dualistic electronic nature of CrO_2. *Phys. Rev. B* **67**, 214419 (2003).

[43] S. P. Lewis, P. B. Allen, and T. Sasaki. Band structure and transport properties of CrO_2. *Phys. Rev. B* **55**, 10253 (1997).